

# THE LNLS BOOSTER SYNCHROTRON DIPOLE MAGNETS

Liu Lin\*, P. Tavares and G. Tosin, LNLS, Campinas, SP, Brazil

## Abstract

The Brazilian Synchrotron Light Laboratory (LNLS) has just constructed and commissioned a 500 MeV booster synchrotron to be used as injector for the 1.37 GeV electron storage ring. The booster has been constructed inside the storage ring, where the constraints in space are very tight. For this reason, the booster dipoles were made as small as possible, i.e., with small curvature radius (magnetic field of 1.6 T) and appreciable fringe field effects. In this report we present the results for the characterization of these magnets and simulation of their effects on the booster optics.

## 1 INTRODUCTION

The Brazilian Synchrotron Light Laboratory (LNLS) has just constructed and commissioned a 500 MeV booster synchrotron to be used as a new injector for the 1.37 GeV electron storage ring [1]. The light source has been operating for users since July 1997 with a 120 MeV LINAC injector. The decision to upgrade the injection energy arose from the need to install small gap insertion devices and also to further increase the stored beam current. To allow the use of the LINAC either to inject into the storage ring or into the booster, the layout of the machines is arranged so that the booster is inside the storage ring and the same straight section in the booster is used for injection and extraction. As expected, these specifications impose strong requirements on the size of the booster and lead us to use strong dipolar magnetic fields, i.e., small radius of curvature to make the dipole magnets as short and as light as possible. The consequences for the beam optics arise in strong fringe field effects which cannot be neglected. The main injector parameters are described in reference [1]. In this report, we concentrate on experimental results on the booster magnet design and characterization as well as its impact on the magnetic lattice design.

## 2 BOOSTER DIPOLE MAGNET OPTICAL MODEL

The model for the dipole magnetic field has to be carefully considered for small rings. Effects from the finite extent of fringe fields or small curvature radius may not be negligible as compared to the effects of the hard-edge model. In the case of the LNLS booster, not only the lattice design had to be re-evaluated in face of the dipole prototype measurement results but also the prototype requirements were re-defined after more accurate lattice design, in an interactive way. Even the orbit length, a zeroth order effect, including magnetic edge fields in

dipoles needs to be taken into account since the RF frequency is already fixed by the storage ring. We have specified for this booster a maximum error of 10 kHz in the rf frequency, which corresponds to a maximum error in each dipole's effective length of 2.5 mm, or  $\pm 1$  lamination thickness. As a by-product of the more careful analysis of the effects of fringe fields on the dipole effective length we have explained a difference of 66 kHz in the 476 066 kHz rf frequency used in the storage ring, which surprised us since its commissioning time. A numerical tracking analysis of the storage ring dipole field measurements has shown that the actual path in each dipole corresponds to a shorter orbit length as compared to the arc with effective length given by the measured integrated field. This effect has been taken into account for the booster and we can indeed operate both machines at exactly the same rf frequency.

The first order focusing effects of dipole edges are well known. In the rectangular hard-edge model the vertical focusing of the beam at entrance and exit edges is given by

$$\frac{1}{f_y} = \frac{1}{\rho} \tan(\beta)$$

where  $\rho$  is the radius of curvature,  $\theta$  is the deflection angle and  $\beta = \theta/2$ . For small  $\rho$ , the contribution from the dipole edge to the vertical focusing can be comparable to that of the quadrupoles in the lattice. For the LNLS booster we have  $\rho = 1.02598$  m and  $\theta = 30^\circ$ , which gives us  $1/f_y = 0.26$  m<sup>-1</sup>. This is about 40% of the value of the strongest quadrupole. In fact, in the booster lattice all quadrupole magnets in the dispersive arc (containing six dipoles) are horizontally focusing. All vertical focusing comes from the dipole edges. The finite extent of the fringe field introduces a correction term to the rectangular dipole vertical edge focusing:

$$\frac{1}{f_y} = \frac{1}{\rho} \tan(\beta - \psi), \quad \psi = K \frac{g}{\rho} \sec \beta (1 + \sin^2 \beta)$$

where  $g$  is the magnet gap and the form factor  $K$  is

$$K = \frac{\int_{-g/2}^{g/2} B_y(z) [B_0 - B_y(z)]}{g B_0^2}$$

$B_y(z)$  is the magnitude of the fringe field on the magnetic midplane at position  $z$  and  $B_0$  is the value of  $B_y(z)$  at the center of the magnet. Numerical integration performed along the electron's trajectory for the measured prototype field gives values for  $K$  ranging from 0.64 to 0.71, depending on the excitation current and shim profile. This corresponds to losing about 20% of the vertical focusing strength as compared to the hard-edge model. Clearly the effect must be taken into account even for first order lattice design. Given the easiness of changing the shim

\* liu@lnls.br

profile at the dipole extremities provided by laser cutting, we decided to shape the vertical focusing of dipole edges according to optimized lattice design calculations. In order to produce a model for the dipole that could represent correctly its field distribution, with finite extent for the fringe field and quadrupolar gradient profile produced by dipole face inclination and shims, a code for numerical tracking of electrons through the measured magnetic field has been developed using Mathematica™. The first order transfer matrix is calculated numerically and the results are compared to the transfer matrix given by a model composed by 63 slices of sector dipoles with field index. There is one big central slice of 20° and 31 small slices to model each edge of 5°. The results agree well and this model is adopted for linear beam optics calculations using MAD[2]. The numerical calculation of the quadrupole gradient is performed at each point at the central trajectory by interpolating the measured field along the perpendicular direction. We have used the measurements of a first prototype as a starting point. In optics matching procedure a scaling factor for the quadrupolar gradient profile (same factor for all slices) was used as a variable parameter. The integrated gradient obtained after lattice optimization has been used as a goal for the next dipole shim profile. The final shim produces an integrated quadrupolar gradient which is larger than the one given by the hard-edge model by 20%.

The sliced dipole model has been implemented in beam optics calculation codes. Different models are used for different excitations of the dipole since the highest currents used already lead into saturation effects (figure 2). In this way the nominal lattice for injection energy is different from the nominal lattice at maximum energy. The lattice transition is done during the energy ramping procedure.

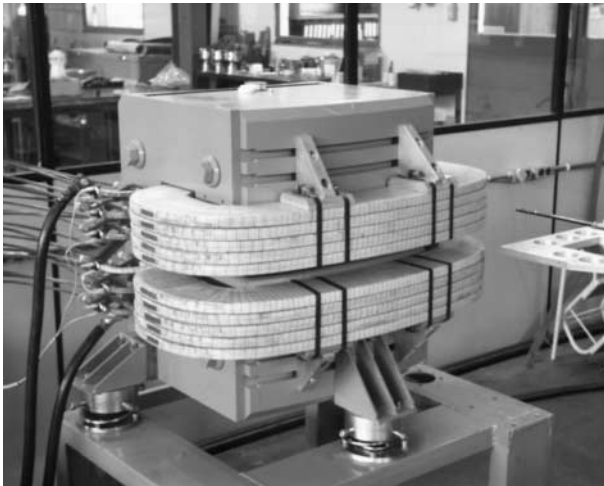


Figure 1: LNLS Booster dipole during measurement using a Hall probe.

### 3 BOOSTER DIPOLE CONSTRUCTION

All booster magnets (as all other DC magnets in the storage ring) are made from laser-cut 1.5 mm thick low-carbon steel laminations and were designed and built at LNLS.

The laminations were stacked in a curved shape, following the orbit, to reduce the magnet weight due the load capacity limit of the crane in the storage ring building. In order to provide the installation of light ports for beam diagnostics and future experiments (with the electron beam and synchrotron radiation), and, to ensure the best repeatability among them, the dipoles are C-type single piece. Care was also taken to guarantee that the physical and the magnetic length match the design specifications so as to provide the expected booster revolution frequency (and the corresponding RF frequency). This required a computer control of the lamination cutting procedure to ensure that, despite of the lamination thickness variations, the dispersion of the overall dipole lengths was the smaller possible. The thickness control was based on the weight of a standard sample cut out from each lamination, resulting in a standard deviation equal 0.35 mm in the twelve dipoles. In fact, the laser cutting procedure is especially convenient for the fabrication of curved dipoles, since it allows the use of tie rods for the assembly of the magnet lamination through the computer controlled holes shift.

Although these dipoles operate in a ramping way (ramping time equal to 1.9 s), no insulation layers were placed between the laminations. The measurements showed that the dynamical magnetic fields is about 1/1000 different of the static field for all the currents.

The coils are water cooled to diminish their sizes, to have a good thermal stability and to obtain a time constant (inductance/resistance) around one second.

The booster dipole main characteristics are shown in the table I.

Table I: Booster dipole main characteristics.

Deflection	30	degree
Bending radius	1.026	m
Gap	36	mm
Maximum current	300	A
Voltage (@ 300 A)	27.7	V
Current density	4.55	A/mm <sup>2</sup>
Maximum magnetic field	16770	Gauss
Inductance	0.13	H
Weight	1175	kg

### 4 MAGNETIC FIELD MEASUREMENTS

Magnetic measurements were performed using a Hall probe along calculated mesh points at the magnetic midplane. The mesh points follow the geometry of the ideal orbit with corresponding points along perpendicular lines on displaced orbits.

Electrons are tracked through this mapped magnetic field assuming that the particle momentum corresponds to and exact 30° bending. The deviation of the trajectories from the ideal path is calculated. The offset at the magnet exit due to asymmetry of the field distribution along the beam orbit leads to amplitudes of about 0.26 mm. The repeatability of measurements for a given current are always better than 1/1000. The main results are shown in table II.

The target installation was managed by a software that after finding the magnetic center using the Hall probe bench, indicated to two theodolites the position to which they need to point.

Table II: Parameters of the booster dipoles calculated by numerical tracking of particles in the measured magnetic field. Statistics over 12 dipoles.

Form Factor	$0.662 \pm 0.002$
Quadupole gradient ( $m^{-1}$ )	$-0.544 \pm 0.001$
Effective length (mm)	$538.6 \pm 0.3$
Offset due to field asymmetry (mm)	$0.26 \pm 0.08$

Figures 2 to 5 show the main measured characteristics of the LNLS booster synchrotron dipoles.

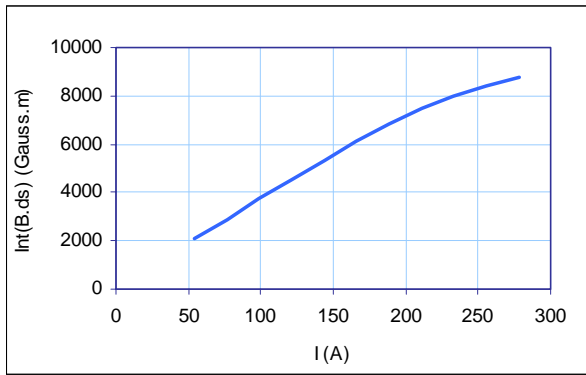


Figure 2: Excitation curve for the booster dipoles.

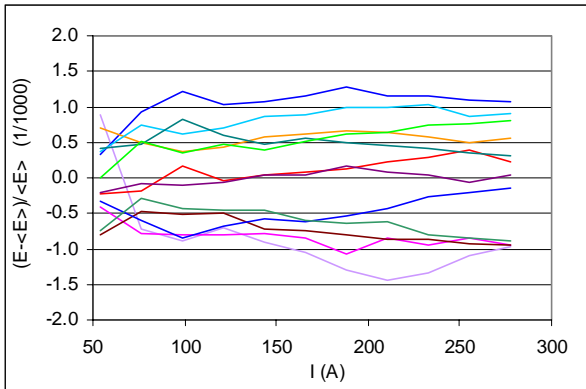


Figure 3: Deviation from average of each individual dipole excitation curve. (Number of dipoles=12).

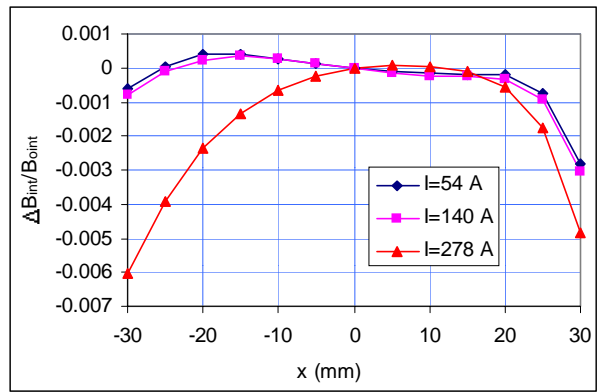


Figure 4: Transverse homogeneity. The curves compare the integrated field along displaced trajectories with the one along the central trajectory for various excitations.

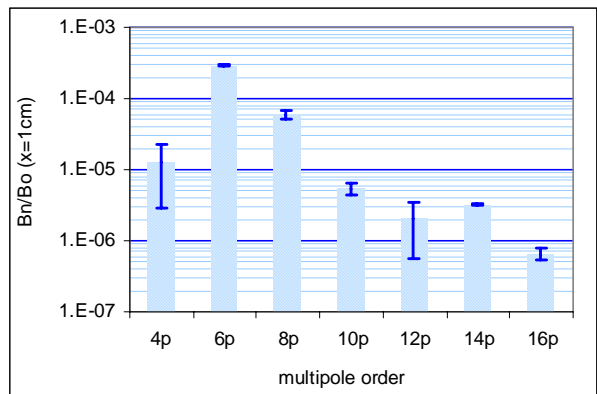


Figure 5: Measured multipole content of the booster dipoles at 500 MeV (278 A). Statistics over 12 dipoles.

## 5 CONCLUSIONS

We have analysed the effect of strong dipole fringe fields on the beam optics. The hard-edge model has been replaced with a sliced model in order to allow setting the correct optics with the desired working point. A code for particle tracking in the dipole magnetic field has been developed to optimize the lamination shimming process and generate the dipole model with finite extent fringe field and quadrupolar gradient profile. The present commissioning results show that the correction in the dipole model was very important since the nominal optics could be easily implemented in the booster.

## 6 REFERENCES

- [1] R.H.A.Farias *et al*, "Commissioning of the LNLS 500 MeV Booster Synchrotron", these proceedings.
- [2] MAD Methodical Accelerator Design.